

L To appear in 5th Edition of Space Physiology and Medicine.

Space Radiation Organ Doses for Astronauts on Past and Future Missions

Francis A. Cucinotta
NASA Lyndon B. Johnson Space Center,
Houston TX 77058

Abstract:

We review methods and data used for determining astronaut organ dose equivalents on past space missions including Apollo, Skylab, Space Shuttle, NASA-Mir, and International Space Station (ISS). Expectations for future lunar missions are also described. Physical measurements of space radiation include the absorbed dose, dose equivalent, and linear energy transfer (LET) spectra, or a related quantity, the lineal energy (y) spectra that is measured by a tissue equivalent proportional counter (TEPC). These data are used in conjunction with space radiation transport models to project organ specific doses used in cancer and other risk projection models. Biodosimetry data from Mir, STS, and ISS missions provide an alternative estimate of organ dose equivalents based on chromosome aberrations. The physical environments inside spacecraft are currently well understood with errors in organ dose projections estimated as less than $\pm 15\%$, however understanding the biological risks from space radiation remains a difficult problem because of the many radiation types including protons, heavy ions, and secondary neutrons for which there are no human data to estimate risks. The accuracy of projections of organ dose equivalents described here must be supplemented with research on the health risks of space exposure to properly assess crew safety for exploration missions.

INTRODUCTION

The health risks to astronauts from space radiation are a major problem for space exploration, perhaps representing a limiting factor on the maximum mission length under current risk acceptance levels. Health risks of concern (NRC, 2005) include cancer, acute radiation sickness, damage to the central nervous system and degenerative effects including cataracts (Cucinotta *et al.*, 2001a) and heart disease (Preston *et al.*, 2004). Cancer risk assessment requires evaluation of organ doses from dosimetry and physical considerations, which are combined with age and gender dependent risk coefficients to project mission risk. The inherent uncertainties in this approach are large (NCRP, 1997; Cucinotta *et al.*, 2001b, 2005; Cucinotta and Durante, 2006) and therefore must be considered in the assessment of the maximum mission duration or the length of the individual's career relative to their participation in one or more space missions. A goal is to use basic knowledge from biophysics to predict risks through the introduction of an explicit dependence on biological factors in risk assessment methodologies. It is worth noting that radiation environments outside and inside of spacecraft have been routinely measured for nearly 30 years (Badhwar, 2004) with a variety of radiation detectors and the particle types and energies, and dynamical range of these particles over the solar cycle are reasonably well understood. However, radiation risk by definition is not measurable and must be understood from basic knowledge of biological damage coupled to human radio-epidemiology data when available. Many important biological questions remain to be addressed before confidence in risk projections for space radiation is improved to a satisfactory level. This will occur only through ground based research with particle accelerators and experimental models of human disease (Cucinotta and Durante, 2006). It is important to accurately assess the organ exposures received by astronauts to assist the planning and goals laid out for this research.

In this paper we review dosimetry data and organ doses received by astronauts on past space missions. We describe NASA's approach to utilize available area and crew specific radiation dosimetry with models of space radiation transport and vehicle and body mass-geometry models to estimate mission specific organ doses, and more

importantly biological dose equivalents. We also discuss comparisons of physical organ dose estimates to results from biodosimetry measurements (Yang *et al.*, 1997, George, *et al.*, 2001; 2004) using the fluorescence in-situ hybridization (FISH) method to score chromosomes aberrations in blood samples collected pre- and post-mission on Mir, space shuttle, and ISS.

SPACE RADIATION ENVIRONMENTS

The sources of radiation in space are the galactic cosmic rays (GCR) and solar particle events (SPE). The GCR consist of high-energy protons, helium nuclei, and heavy nuclei with energies extending to more than 10 GeV/amu, and SPEs are largely protons with energies up to a few hundred MeV with a small helium and heavy ion component (NCRP, 2000). The GCR interaction with the Earth's atmosphere and magnetic field creates the trapped protons and electrons belts important for missions in low-Earth orbit (LEO). The sun's magnetic field modulates the GCR over an approximately 11-year cycle with a more than a factor of two change in flux rates at the highest conditions called solar minimum from lowest point in the cycle called solar maximum. This variation is described by the solar modulation parameter, $\Phi(\text{MV})$ which is used in the solution of the time-dependent Fokker-Planck diffusion equation for GCR transport inside the heliosphere (Badhwar, 1997). Past values and a statistical projection into the future (Kim *et al.* 2006) are shown in **Figure 1**. Solar particle events are more likely to occur at solar maximum as illustrated in the lower panel **Figure 1** where the dates of the largest SPE's with fluences protons of 30 MeV of at least 10^8 protons per cm^2 are shown over the last 50-years.

The amount of radiation received by astronauts depends on several factors including orbital inclination, altitude, position in the solar cycle, and mission duration. The energy spectrum of each source determines their range in shielding material and the human body. Trapped electron energies extend to a few MeV with ranges less than about 1-cm in water and include a small bremsstrahlung component capable of reaching larger depths. Trapped protons have energies extending to several hundred MeV, however more than 90% of the

flux is from particles with ranges less than 1 cm in water. A small high-energy component is capable of penetrating crew compartments and tissues producing secondary neutrons and highly ionizing hydrogen, helium, and heavy ions (Cucinotta *et al.*, 1996). In contrast to trapped radiation, incident GCR in LEO are dominated by relativistic particles with energies of 1 GeV/amu or more as the Earth's magnetic field provides shielding from the lower energy components. Relativistic ions have large ranges and undergo numerous nuclear reactions in shielding causing a build-up of secondary particles including neutrons, hydrogen and helium ions, heavy ions, and mesons. The flux of secondary particles increases for materials with high atomic mass constituents, such that hydrogen is the most effective shielding material and in-fact materials with heavier constituents such as steel or lead significantly increase radiation doses (Wilson *et al.*, 1995).

RADIATION DOSE LIMITS FOR ASTRONAUTS

The absorbed dose, D , of radiation represents the amount of energy deposited in bulk material and is expressed in units of joules per gram (J/g) which is given the special name of Gray (Gy) (1 Gy = 100 rad). For particle radiation, the absorbed dose is expressed as the product of the fluence of particles (the number per unit area), F and the linear energy transfer (LET), L as

$$(1) \quad D = F L$$

The approach use for estimating risks in humans from atomic nuclei is to consider experimental models to estimate relative effectiveness factors comparing nuclei to γ -rays. These factors are combined with human data for γ -rays to predict risks for nuclei. The relative biological effectiveness (RBE), defined as the ratio of the dose of a reference radiation (usually assumed as γ -rays) to the radiation under study that will produce an equal level of effect (for a given experimental observation), is the relative factor used most often as defined (Butts and Katz, 1967). Values of RBE extending over more than two orders of magnitude have been observed that are dependent on the biological end-

point, cell or animal models, the dose and dose-rate, and the type of radiation (NCRP, 2000). Other limitations of the RBE approach include that for practical or financial reasons, RBE's are not determined for many of the types of radiation or doses and dose-rates of interest for radiation protection. The diversity of particle types that occur in space requires a large number of measurements to understand a detailed RBE-LET relationship. It is possible that high LET radiation produces effects that are qualitatively different from photons and therefore could not in principle be related to an equivalent dose of photons. For these and other reasons there are important limitations expected in using a RBE approach for risk assessment in space, however an alternative has not been accepted at this time.

National and international radiation protection policy committees make recommendations on values of RBE's to be used for assessing risks to humans. The approach taken by these committees has been to introduce an LET-dependent radiation quality factor, $Q(L)$ or radiation-weighting factor, w_R that represent knowledge of RBE's at low doses and dose-rates. The role of the committee has been to determine the most appropriate RBE data to assign values of $Q(L)$. The current values of $Q(L)$ peak at a value of 30 for a LET value of 100 keV/ μm and decline and higher values of LET (NCRP, 2000). The point dose equivalent is defined

$$(2) \quad H = DQ(L)$$

For evaluating organ dose or organ dose equivalent, the dose and dose equivalent are summed over the LET spectra at the tissue of interest as described below.

NASA imposes short-term and career dose limits, which have distinct purposes. Short-term limits are intended to prevent the occurrence of any clinically significant health risk. And career limits are intended to limit the increased risk of cancer to an acceptable level. Early radiation effects are deterministic in nature and occur only above dose thresholds, usually after a significant fraction of cell loss in a tissue. **Table-1a** lists the short-term dose limits followed by NASA. Because very little age- or gender-differences are seen

for early effects, these limits are age- and gender-independent, and are expected to be conservative because most solar proton events deliver doses at a low to modest dose-rate (<0.3 Gy/hr). Recent information suggests that cataract risks from space radiation are linear with GCR dose (Cucinotta *et al.*, 2001a), with no apparent threshold, and caused by genetic damage leading to aberrant cellular differentiation of lens epithelial cells (Blakely *et al.*, 1999; Worgul *et al.*, 1989). However, questions on the definition of clinical significance and the progression of cataracts with age must be addressed for the proper risk assessment for cataracts.

Late effects, such as cancer, are stochastic in nature and some level of risk is incurred even at low doses. The earliest dose limits used by NASA originated from recommendations from the National Academy of Sciences using the criteria of a doubling dose over a 20-yr period for fatal cancer for males of age 35-yr as a basis (NAS, 1970). In 1989, the National Council on Radiation Protection and Measurements (NCRP) issued their Report No. 98 (NCRP, 1989) that made recommendations of gender- and age-dependent career dose limits using a risk limit of a 3% increase in cancer fatality. This upper level of acceptable risk was chosen by comparing to rates of occupational death in the less-safe industries and noting that the average years of life loss from radiation induced cancer death (about 15 years) would be less than that of other occupational injuries (NCRP, 1989; Fry and Nacthwey, 1988). In the 1990's the continued maturation of the atomic-bomb survivor data and the re-evaluation of the doses received by the survivors led to further reductions in estimated cancer risks. Recommendations from the NCRP (NCRP, 2000), while keeping the basic philosophy of their earlier report including a 3% maximum risk level, result in a lower dose limits than those recommended in 1989 (NCRP, 1989). Continued follow-up of the atomic-bomb survivor is used to refine risk estimates for cancer and non-cancer diseases (Preston *et al.*, 2003).

NASA has made several recent changes to the implementation of career limits for fatal cancer. The quantity excess lifetime risk (ELR) has been abandoned because of the difficulties in comparing ELR to other mission risks, and because in-fact it is poorly defined mathematically, especially when competing risks are significant (Vaeth and

Pierce, 1990). Instead, NASA is using the quantity risk of exposure induced death (REID) as a basis for dose limits. Values of REID are generally 10 to 20% higher than ELR, and more importantly the REID correctly describes competing risks. Because of the large uncertainties in projecting the risk of late effects from heavy ions (Cucinotta *et al.* 2001; Cucinotta and Durante, 2006), NASA applies career limits with a concurrent evaluation of the 95% confidence level (CL) in the uncertainties that enter into the risk calculations (NCRP, 1997; Cucinotta *et al.*, 2001). Failure to meet the 95% CL initiates a more stringent set of risk evaluations and mitigation measures, albeit it is not imposed as an absolute mission exclusion criteria. **Table 1B** shows dose limits proposed for lunar missions at NASA using the REID criteria of a 3% limit. Also shown are calculations of the average life-loss expected if a cancer fatality would occur that are estimated from human data for low LET radiation exposure.

SPACE ORGAN DOSE EVALUATION

The approach used at NASA to determine organ doses is to utilize available radiation dosimetry from each mission in conjunction with space radiation transport models to estimate organ dose, dose equivalent, and particle fluence. Area measurements of doses are considered first and assumed to be made-up of two components; the GCR and trapped protons including each secondary components. Shielding amounts are described by the areal density, x , in units of g/cm^2 , which represents the physical thickness, t in units of cm times the material density, ρ , in units of g/cm^3 , or $x = \rho t$. Areal density is the preferred quantity for scaling physical parameters describing radiation transport, and for comparison of the shielding effectiveness of different materials on a common mass-scale. The GCR contribution varies slowly with the amount of shielding and the trapped proton contribution varies quite strongly becoming negligible at large shielding depth ($>20 \text{ g}/\text{cm}^2$). This observation is used in a re-normalization procedure of transport code results to the available mission and astronaut specific dosimetry described next.

The main source of passive dosimetry data are thermoluminescence dosimeters (TLD) that are worn by each astronaut during his or her mission. In some cases CR-39 plastic

track detectors have been included in the passive dosimetry packages (Benton, 1986). Additional information is obtained by TLD's that are mounted throughout space vehicles such as the space shuttle, space station Mir, and the International Space Station (ISS) to survey the variation of point dose dependencies from shielding variations.

Tissue equivalent proportional counters (TEPC's) have been flown on some space shuttle missions and on the Mir and ISS. TEPC's provide time dependent data and a method to estimate the individual contributions from the GCR and trapped proton doses because of the strong geographical dependence of the trapped protons. **Figure 2** shows the γ -spectrum from a TEPC flown next to the phantom torso experiment on ISS Expedition-2. It can be seen that GCR flux dominates the exposure in a well shielded location such as near the human body. Radiation protection protocols use LET and not γ in the definition of radiation quality factors and is important to understand the differences between these two quantities (Nikjoo *et al.*, 2002). LET and γ deviate because LET represents bulk energy loss by particles, while γ represents the energy deposited in a small microscopic volume usually taken as a sphere of 1 micron diameter. **Figure 3** shows TEPC measurements from STS-56 for the GCR components and calculations using the HZETRN codes (Wilson *et al.*, 1990) and a TEPC response model (Cucinotta *et al.*, 2000a; Nikjoo *et al.*, 2000) that accounts for the differences between γ and LET-spectra. The main differences that occur between LET and γ -spectra are due to the escape of a portion of the energy loss by electrons out of the sensitive volume, the effects of energetic electrons produced in the walls of the detector, which lead to anomalous events, and the high- γ resolution of a TEPC (Badhwar and Cucinotta, 2000). These effects are reasonably understood with TEPC's over-estimating of the average quality factors for trapped protons and under-estimating average quality factors for GCR. However, TEPC data can be used to validate models used to predict organ dose equivalents when models of TEPC response functions are coupled to space transport models, albeit not for a direct measurement of mission quality factors.

The NASA computer code, HZETRN uses models space radiation environment as a boundary condition for a Boltzmann equation solver describing radiation transport in

materials (Wilson *et al.*, 1991). The large number of nuclear fragmentation reactions requires an extensive physical interaction data-base and the quantum multiple scattering (QMSFRG) model provides an accurate data base agreeing with over 85% of the measured heavy ion cross sections with less than $\pm 25\%$ error (Cucinotta *et al.*, 2006). In **Figure 4** we show contributions of different particle types to space exposures on ISS (Cucinotta *et al.*, 2000a). The H and He components include the tertiary contributions produced by neutrons which increase with shielding. Heavy ions are seen to make up a major fraction of the dose equivalent due to their higher quality factors at small to medium shielding depths (≤ 20 g/cm²), and neutrons make dominant contributions at larger depths.

As shown in **Tables 2** and **3**, these models reproduce space flight measurements for point dose and dose equivalent, and organ doses and dose equivalents (Badhwar *et al.*, 2001, Yasuda *et al.*, 2000) to a high degree of accuracy. However for the official astronaut records of organ dose equivalent and the risk projection data-base at NASA, the re-normalization procedure described next ensures that the results match the dosimetry of record, and represent a further improvement in accuracy over the absolute comparisons shown in **Tables 2** and **3**.

A two-dimensional matrix, corresponding to the vehicle and tissue shielding amounts, is computed for the flux of ion j of energy, E (units of MeV/u) at depth x (units of g/cm²) in spacecraft shielding, and depth z (units of g/cm²) in tissue denoted as $\phi_j(E, x, z)$ (units of ions per cm² per MeV/u). Matrix of values of the absorbed dose, TLD-dose, and dose equivalent using the NASA HZETRN computer transport code are then evaluated as

$$(3) \quad D(x, z) = \sum_j \int dE \phi_j(E, x, z) S_j(E)$$

$$(4) \quad D_{TLD}(x, z) = \sum_j \int dE R_{TLD}(Z_j, E) \phi_j(E, x, z) S_j(E)$$

$$(5) \quad H(x, z) = \sum_j \int dE \phi_j(E, x, z) S_j(E) Q(S_j(E))$$

where $S_j(E)$ is the ion linear energy transfer, which depends on kinetic energy and mass and charge number, Z_j . The TLD dose considers a response function, $R_{TLD}(Z,E)$ that represents the reduced efficiency of TLD's to high LET components. TLD's underestimate the trapped proton dose by about 5% and the GCR dose by about 10% (Yasuda, *et al.*, 2000). Radiation transport models provide an estimate of the correction of the dose measured by the TLD to the actual absorbed dose. Organ doses for a tissue T are averaged over shielding at a spacecraft location, n as

$$(6) \quad D_T(n) = \sum_j \sum_x a_x \sum_z b_z \int dER_{TLD}(Z_j, E) \phi_j(E, x, z) S_j(E)$$

where a_x and b_y are shielding fractions of equal solid angle intervals from a shielding model for the spacecraft or organ. The ‘‘point’’ dose, D_{pt} is defined by Eq. (6) for $z=0$.

The model organ or tissue dose consisting of GCR and trapped proton component at a spacecraft location, n , are written as

$$(7) \quad D_T(n) = D_{T,GCR}(n) + \alpha D_{T,trap}(n)$$

The first re-normalization of the model determines the coefficient, α by assuming the error in the baseline model and measurement is dominated by inaccuracies in the trapped proton environment. Using mission specific area dose measurements compared to the model point-dose estimates at the dosimeter area shielding we choose the normalization constant, α , to minimize χ^2

$$(8) \quad \chi^2 = \sum_n |D_{TLD}(n) - (D_{pt,GCR}(n) + \alpha D_{pt,trap}(n))|^2$$

In applying eq.(8) measurements at 6 locations in the space shuttle and 5 locations in the ISS service module where passive dosimetry are located are used. Since an astronaut's

location is not precisely known during the mission, we make comparisons of dose values at fixed dosimeter locations to understand possible variations within a vehicle. The second re-normalization of the model estimated doses is made to the dose recorded by the badge for each crew-member to determine the parameter, β , from

$$(9) \quad D_{\text{badge}} = \beta \sum_n C_n D_{\text{TLD,skin}}(n)$$

where the C_n are fractions of time at specific locations used to sample from the variations in the internal spacecraft radiation environment throughout a spacecraft. The organ dose equivalent is then given by

$$(10) \quad H_T = \beta \sum_n C_n [H_{T,GCR}(n) + \alpha H_{T,trap}(n)]$$

The effective dose (ICRP, 1991) is defined as an average of organ dose equivalents using the tissue weighting factors, w_T , as written

$$(11) \quad E_T = \sum w_T H_T$$

The tissues weighting factors (ICRP, 1990) are estimates of the average contribution from specific tissues to the overall cancer burden with the major sites including the blood forming organs, stomach, bladder, breast, lung, and gonads. The tissue weighting factors are defined to reflect the total detriment from radiation exposure, which includes consideration of the years of life-loss expected for different types of cancer deaths, cancer morbidity and hereditary effects, however any age or gender dependence is ignored. For the astronaut's official records, the effective dose is not used and instead risks for solid cancer and leukemia are calculated individually using age and gender-specific risk coefficients, and 95% confidence levels determined using the methods described by Cucinotta *et al.* (2001b, 2005, 2006).

Vehicle shielding mass geometry models are used to assess the predictions of radiation

transport codes to the area measurements. Shielding models exist for the Space shuttle, the Mir space station, and the ISS. These models contain some inaccuracies due to their method of construction, for e.g., the use of scaling assumptions for distinct materials to an equivalent aluminum thickness, and changes in the local interior environment from mission to mission due to specific flight manifests. However, in the re-normalization approach to mission and astronauts specific dosimetry described above, such inaccuracies are minimized. In the transport calculations the astronaut is placed at the locations of the area dosimeters and an approximate average location is defined for the final dose estimates. In actuality only a small variation in the organ dose equivalent is found at the different locations within a vehicle, albeit the point dose variations (no tissue shielding) can be as much as 50%. One effect that is not accounted for in this procedure is the astronaut orientation within the vehicle, which can lead to non-negligible variations for trapped proton doses (Wilson *et al.*, 1995). However because the vehicle and astronaut are in changing orientations throughout the mission relative to the orientation of the trapped protons along the so-called pitch angle distribution (NCRP, 2000), we assume an average orientation in the calculations. A computerized anatomical model (CAM) of the human body (Billings *et al.*, 1973) is used in this procedure to allow for predictions of organ specific quantities including the skin dose at the chest and the lens dose.

DOSES ON SPACE MISSIONS

In **Table-4** and **Figure-5** and we show the average and individual effective dose-rates, respectively, for all astronauts from all NASA Missions (through 2004). These results use records of passive dosimetry worn on all NASA missions (excluding the Mercury I and II missions where dosimetry was not utilized), and estimates of tissue absorption and average quality factors from flight spectrometers and radiation transport codes. The effects of the 11-yr solar cycle can be seen in the changes in dose-rates shown in **Figure-6**. Also, dose-rate increase at higher altitudes due to longer sampling of the Earth's trapped radiation belts, with the highest dose-rate occurring on the Hubble telescope launching and repair missions with altitudes near 600 km. Average quality factors range from about 1.6 to 3.5 with the highest values occurring for GCR dominated missions such

as the Apollo missions. For the deep space Apollo missions, the GCR dominated astronaut doses with a small contribution from the trapped belts. The International Space Station (ISS) and Mir missions were in a 51.6-degree inclination with altitudes ranging from about 340 to 400 km have led to effective dose-rates will range from 0.4 to about 1 mSv/day over the course of the solar cycle. Organ dose equivalents are made-up of more than 80% contributions from GCR for most missions. US participation on the Mir missions occurred near solar minimum, while the results in **Figure-6** for the ISS Expeditions 1-10 are at or near solar maximum resulting in a lower dose-rate. The large number of medium size SPE's occurring past the most recent solar maximum in 2000 in effect reduced ISS crew exposures as the solar modulation parameter has remained at higher values as solar minimum in late 2006 was approached.

Doses received by crews during extra-vehicular activities (EVA) are a particular concern because there is much less shielding outside a vehicle compared to the interior. NASA has scheduled EVA's to occur outside the south Atlantic anomaly region of the trapped proton belts and outside the higher magnetic latitudes of the Earth's magnetic fields. Mission planners have agreed to schedule the majority of EVA's during these orbits, which occur over about a 12- hour time period each day. Although data on EVA doses is not generally available, a comparison of total mission doses for astronauts performing space-walks relative to other astronauts on the same mission that did not participate in EVA's is possible. This comparison is shown in **Figure-7** and provides strong evidence that proper EVA scheduling can be effectively used to ensure EVA doses are negligible.

BIODOSIMETRY ON LONG-TERM SPACE MISSIONS

Biodosimetry offers an alternative method to consider space radiation organ doses that offers advantages over physical dosimetry. Pros to biodosimetry include providing a method to include the self-shielding of the body, individual sensitivity, and because chromosomal damage is known to provide good response to high LET heavy ions and neutrons, which is not true for TLD measurements or many other forms of physical dosimetry. The self-shielding is important because of the loss and gains of distinct

particle types including energy or LET changes as radiation passes through tissue, which can not be accounted for by a measurement on the body surface. In some cases astronauts for practical or other reasons do not wear the badges for portions of a mission, which is not a limitation with a blood sample. Cons to biodosimetry include statistical limitations that occur based on the blood sample size, especially at low doses (<50 mSv), and possible anomalies that may occur in the sample including poor growth simulation and the presence of clonal aberrations (George *et al.*, 2004). For long missions, it is possible that a percentage of damaged cells are lost before the post-flight sample is analyzed.

At NASA biodosimetry is performed for all long duration missions using the method of fluorescence in-situ hybridization (FISH) or whole cell chromosomal painting. Three large chromosomes, typically chromosomes 1, 2 and 4 are painted with unique colors and all other chromosomes are counter-stained with a dapi blue chemical (George *et al.* 2004). Aberrations between chromosomes including translocations, dicentrics, and complex aberrations are then scored. A pre-flight sample is taken at about 90 days before the mission and a baseline and dose-response calibration curve for gamma-rays is determined. The post-flight yield of aberrations, Y_f is then compared to the pre-flight baseline, Y_i and dose calibration curve to estimate a biological dose. Here a weighted linear regression model is fit the pre-flight sample exposed to gamma-rays at low doses, $Y_i=A+BD$. The post-flight biological dose is then estimated as $D_{post}=(Y_f-A)/B$. **Figure 8** shows a comparison of the biological doses versus effective dose estimates for astronauts on Mir, a high-altitude Hubble repair mission, and several ISS missions. The left panel show the biological dose estimate based on the individuals pre-flight calibration curve to gamma-rays, and the right hand panel is the comparison using pre-flight calibration averaged over the population of astronauts undergoing biodosimetry evaluation. Individual variations to the exposure are clearly evident in the results.

FUTURE CONSIDERATIONS

The results described here show that astronaut organ dose exposures are now well described by space radiation transport models with an accuracy of better than $\pm 15\%$.

However, for outpost missions to the moon lasting about 180 days or Mars missions expected to last from 600-1000 days, effective doses from GCR will be much higher (**Table-5**) than past space missions because of the absence of the magnetic protection provided by the Earth from lower energy GCR components and longer duration of the missions. In addition, a significant probability would exist for one or more large solar particle events. Dose limits have not been defined for a Mars missions, and await both new knowledge needed for risk assessment, and considerations of what is the acceptable level of risk for such missions. Using the recent NCRP risk estimates and organ dose equivalents we can estimate that no NASA astronaut has achieved a point estimate of lifetime risk (REID) of more than 1% cancer fatality. However, long-term deep space missions will incur risks of 3 to 5 % and estimates of uncertainties in risk estimates (Cucinotta *et al.*, 2001b; Cucinotta and Durante, 2006) show 95% confidence levels exceeding a 10% risk. Also, risks to the central nervous system will be of a higher concern for a Mars mission than past missions in low Earth orbit (NCRP, 2000). Understanding the biological effects of such exposures and developing effective counter-measures is a major endeavor and is the focus of current research efforts at NASA. These problems are a major scientific challenge, requiring the dedication of the biomedical research community in the United States and other nations with interest in space travel to realize the necessary solutions.

ACKNOWLEDGEMENTS

Special appreciation is extended to Bill Atwell, Myung-Hee Kim, and Kerry George in the preparation of this report. The memories of our colleagues, Dr.'s Stuart Natchwey, Tracy Yang and Gautam Badhwar are noted in our summary of past space results.

REFERENCES

Badhwar, G.D., Spaceflight Validation of Material Shielding Properties. In: NASA Workshop on Shielding Strategies for Human Space Exploration. Eds. Wilson, J.W., Miller, J., Konradi, A., and Cucinotta, F.A. NASA-CP-1997-3360, 1997.

Badhwar, G.D., Cucinotta, F.A.: A Comparison of Depth Dependence of Dose and Linear Energy Transfer Spectra in Aluminum and Polyethylene. *Radiat. Res.* **153**, 1–8, 2000.

Badhwar, G.D., W. Atwell, F. F. Badavi, T. C. Yang, And T. F. Cleghorn: Space Radiation Absorbed Dose Distribution in a Human Phantom. *Radiat. Res.* **157**, 76-91, 2002.

Benton, E.V.: Summary of Radiation Dosimetry Results on the U.S. and Soviet Manned Spacecraft. *Adv. Space Res.* **6**, 315-328, 1986.

Billings, M.P., Yucker, W.R., Heckman, B.R.: Body Self-Shielding Data Analysis, McDonald Douglas Astronautics Company West, MDC-G4131, 1973.

Blakely, E.A., Bjornstad, K.A., Chang, P.Y., McNamara, M.P., Chang, E., Aragon, G., Lin, S.P., Lui, G., and Polansky, J.R.: Growth and differentiation of human lens epithelial cells in vitro on matrix. *Inv. Opth. & Vis. Sci.* **41**, 3898-3907, 1999.

Butts, J.J. and Katz, R.: Theory of RBE for Heavy Ion Bombardment of Dry Enzymes and Viruses. *Radiat. Res.* **30**, 855-871, 1967.

Cucinotta, F.A., J.W. Wilson, J.L. Shinn, F.F. Badavi, and G.D. Badhwar: The Effects of Target Fragmentation on LET Spectra from Space Radiation. *Radiat. Meas.* **26**, 923-934, 1996.

Cucinotta, F.A., Nikjoo, H., and Goodhead, D.T.: Radial Distribution of Energy Imparted in Nanometer Volumes from HZE Particles. *Radiat. Res.* **153**, 2000a.

Cucinotta, F.A., Wilson, J.W., Williams, J.R., Dicello, J.F.: Analysis of Mir-18 Results for Physical and Biological Dosimetry: Radiation Shielding Effectiveness in LEO. *Radiat. Meas.* **31**, 181-191, 2000b.

Cucinotta, F.A., Manuel, F.K., Jones, J., Izsard, G., Murrey, J., Djojonegro, B., and Wear, M. Space Radiation and Cataracts in Astronauts. *Radiat. Res.* **156**, 460-466, 2001a.

Cucinotta, F.A., Schimmerling, W., Peterson, L.E., Wilson, J.W., Badhwar, G.D., Saganti, P., and Dicello, J.F.: Space Radiation Cancer Risks and Uncertainties for Mars Missions. *Radiat. Res.* **156**, 682-688, 2001b.

Cucinotta, F.A., Kim, M.Y., and Ren, L: Managing Lunar and Mars Mission Radiation Risks Part I: Cancer Risks, Uncertainties, and Shielding Effectiveness. NASA/TP-2005-213164.

Cucinotta, F.A., and Durante, M.: Cancer Risk from Exposure to Galactic Cosmic Rays: Implications for Space Exploration by Human Beings. *The Lancet Oncology* **7**, 431-435, 2006.

Cucinotta, F.A., Wilson, J.W., Saganti, P., Hu' X., Kim, MY, Cleghorn' T., Zeitlin, C., Tripathi, R.K., Isotopic Dependence of GCR Fluence Behind Shielding. *Radiat. Meas.* **41**, 1235-1249, 2006.

Fry, R.J.M., and Nachtwey, D.S.: Radiation Protection Guidelines for Space Missions. *Health Phys.* **55**, 159-163, 1988.

George, K., Wu, H., Durante, M., Willingham, V., and Cucinotta, F.A.: Chromosome Aberrations in Blood Lymphocytes of Astronauts after Space Flight. *Radiat. Res.* **156**, 731-738, 2001.

George, Durante, M., Willingham V. and Cucinotta, F.A.: Chromosome Aberrations of Clonal Origin are Present in Astronauts' Blood Lymphocytes. *Cytogenetics and Genome Res.* **104**, 245-251, 2004.

International Commission on Radiological, Recommendations of the International Commission on Radiological Protection. ICRP Publication 60, Pergamon Press, Oxford, 1990.

Kim, M.Y., Wilson, J.W., and Cucinotta, F.A.: A Solar Cycle Statistical Model for the Projection of the Space Radiation Environment. *Adv Space Res* **37**, 1741-1748, 2006.

National Council on Radiation Protection and Measurements. Guidance on Radiation Received in Space Activities NCRP Report No. 98. National Council on Radiation Protection and Measurements, Bethesda MD, 1989.

National Council on Radiation Protection and Measurements, Uncertainties in fatal cancer risk estimates used in radiation protection, NCRP Report 126, Bethesda MD, 1997.

National Council on Radiation Protection and Measurements, Recommendations of Dose Limits for Low Earth Orbit. NCRP Report 132, Bethesda MD, 2000.

National Academy of Sciences National Research Council, Radiation Protection Guides and Constraints for Space-Mission and Vehicle-Design Studies Involving Nuclear System, Washington D.C., 1970.

Nikjoo, H., Khvostunov, I.K., Cucinotta, F.A.: The Response of (TEPC) Proportional Counters to Heavy Ions. *Radiat. Res.* **157**, 435–445, 2002.

Preston, D.L., Shimizu, Y., Pierce, D.A., Suyumac, A., and Mabuchi, K.: Studies of Mortality of Atomic Bomb Survivors. Report 13: Solid Cancer and Noncancer Disease Mortality: 1950–1997. *Radiat. Res.* **160**, 381-407, 2003.

Vaeth, M., and Pierce, D.A.: Calculating Excess Lifetime Risk in Relative Risk Models. *Environ. Health Per.* **87**, 83-94, 1990.

Wilson J.W., Townsend, L.W., Schimmerling, W., Khandelwal, G.S., Khan, F., Nealy, J.E., Cucinotta, F.A., Simonsen, L.C., Norbury, J.W., Transport Methods and Interactions for Space Radiations. RP1257, NASA, Washington D.C., 1991.

Wilson, J.W., Kim, M.; Badavi, F. F.; Thibeault, S. A.; Cucinotta, F.A., Shinn, J.L., and Kieffer, R., Issues in Protection From Galactic Cosmic Rays. *Radiat. Environ. Biophys.* **34**, 217-222, 1995.

Worgul, B.V., Merriam, G.R., Mededovsky, C., and Brenner D.J.: Accelerated Heavy Particles and the Lens III Cataract Enhancement by Dose Fractionation. *Radiat. Res.* **118**, 93-100, 1989.

Yang, T.C., George, K., Johnson A.S., Durante, Federenko, B.S.: Biodosimetry Results from Space Flight Mir-18. *Radiat. Res.* **148**, 17-23, 1997.

Yasuda, H., Badhwar, G.D., Komiyama, T., and Fujitaka, K.: Effective Dose Equivalent on the Ninth Shuttle-Mir Mission (STS 91). *Radiat. Res.* **154**, 705-713, 2000.

Table-1a. Short-term dose limits (in Gy) for preventing deterministic radiation effects for Space Activities in low Earth orbit (LEO) (NCRP, 2000).

<i>Organ</i>	<i>30 day limit</i>	<i>1 Year Limit</i>
Eye	1.0 Gy-Eq	1.5 Gy-Eq
Skin	2.0	3.0
BFO	0.25	0.5

Table-1b. Example career effective dose limits in units of Sievert (mSv) corresponding to a REID of 3% for 1-year missions and projection of average Life-loss for an exposure induced death for radiation carcinogenesis (1 mSv= 0.1 rem).

<i>Age, yr</i>	<i>Career effective dose limits in units of Sievert (mSv) for 1-year missions (Ave Life Loss).</i>	
	<i>Males</i>	<i>Females</i>
25	520 (15.7)	370 (15.9)
30	620 (15.4)	470 (15.7)
35	720 (15.0)	550 (15.3)
40	800 (14.2)	620 (14.7)
45	950 (13.5)	750 (14.0)
50	1150 (12.5)	920 (13.2)
55	1470 (11.5)	1120 (12.2)

Figure-2: Comparison of HZETRN/QMSFRG model to flight measurements on NASA space shuttle and Russian Mir space station. Shielding locations represent locations within the space shuttle or Mir station where TEPC's were located. For the STS-81 and STS-89 missions TEPC's were embedded within polyethylene or aluminum spheres of different thicknesses and stowed inside the payload bay of the space shuttle (Badhwar and Cucinotta, 2000).

Mission	DATE	Inclination	Altitude	Shielding	Dose, mGy/d			Dose Eq., mSv/d		
					Measured	Theory	%Difference	Measured	Theory	%Difference
STS-40	1991	39	293	Dloc2	0.052	0.048	7.7	0.13	0.16	-23.1
STS-49	1992	28.5	358	Dloc2	0.05	0.048	4.0	0.127	0.155	-22.0
STS-51	1993	28.5	296	Payload Bay	0.044	0.048	-9.1	0.144	0.154	-6.9
STS-57	1993	57	298	Payload Bay	0.113	0.109	3.5	0.422	0.434	-2.8
STS-57	1993	57	298	DLOC-2	0.138	0.11	20.3	0.414	0.37	10.6
Mir-18	1995	51.6	390	P	0.142	0.141	0.7	0.461	0.526	-14.1
STS-81	1997	51.6	400	0-sphere	0.147	0.135	8.2	0.479	0.521	-8.8
STS-81	1997	51.6	400	Poly 3-in	0.138	0.138	0.0	0.441	0.400	9.3
STS-81	1997	51.6	400	Poly 5-in	0.129	0.118	8.5	0.316	0.368	-16.5
STS-81	1997	51.6	400	Poly 8-in	0.128	0.113	11.7	0.371	0.323	12.9
STS-81	1997	51.6	400	Poly 12-in	0.116	0.111	4.3	0.290	0.298	-2.8
STS-89	1998	51.6	393	0-sphere	0.176	0.148	15.8	0.561	0.614	-9.4
STS-89	1998	51.6	393	Al 3-in	0.167	0.159	4.8	0.445	0.488	-9.7
STS-89	1998	51.6	393	Al 7-in	0.149	0.161	-8.1	0.529	0.617	-16.6
STS-89	1998	51.6	393	Al 9-in	0.171	0.162	5.3	0.492	0.541	-10.0

Table 3a. Comparison of measured organ dose equivalent for STS-91 mission by Yasuda *et al.* (2000) using combined CR-39/TLD method to HZETRN/QMSFRG space transport model.

Tissue	<i>Organ Dose Equivalent, mSv</i>		
	Measured	Std. Error	HZETRN/QMSFRG
Skin	4.5	0.05	4.7
Thyroid	4.0	0.21	4.0
Bone surface	5.2	0.22	4.0
Esophagus	3.4	0.49	3.7
Lung	4.4	0.76	3.8
Stomach	4.3	0.94	3.6
Liver	4.0	0.51	3.7
Bone marrow	3.4	0.40	3.9
Colon	3.6	0.42	3.9
Bladder	3.6	0.24	3.5
Gonad	4.7	0.71	3.9
Chest	4.5	0.11	4.5
Remainder	4.0	0.57	4.0
Effective dose	4.1	0.22	3.9

Table 3b. Comparison of small active dosimetry data from the ISS Increment-2 Phantom Torso Experiment in comparison to the calculations from the HZETRN/QMSFRG model.

SMADOS	Measurement time during July 26-August 1, 2001 and August 7-11, 2001 (day)	Trapped radiation (mGy/d)		GCR (mGy/d)		Total dose rate (mGy/d)		Difference
		Meas.	Calc.	Meas.	Calc.	Meas.	Calc.	
BRAIN	10.211	50.7	66.3	75.8	77.0	126.5	143.3	13.3%
THYROID	10.028	61.6	71.7	73.9	76.6	135.5	148.3	9.4%
HEART	11.149	53.5	61.4	75.3	76.0	128.8	137.4	6.7%
STOMACH	11.045	50.4	56.5	75.8	76.7	126.2	133.2	5.5%
COLON	10.349	55.4	55.5	72.8	75.9	128.2	131.4	2.5%

Table-4. Average dose (D) or dose-rate recorded by dosimetry badge and estimates of the effective doses, E received by crews in NASA programs through 2004.

<i>NASA Program</i>	<i>No. Crew</i>	<i>D, mGy</i>	<i>E, mSv</i>	<i>D-rate, mGy/d</i>	<i>E-rate, mSv/d</i>
Mercury	6	0.1	0.15	0.3	0.55
Gemini	20	1.3	2.2	0.49	0.87
Apollo	33	4.1	12.0	0.43	1.2
Skylab (50 deg x 430 km)	9	40.3	95.0	0.71	1.4
ASTP (50 deg x 220 km)	3	1.1	2.3	0.12	0.26
STS					
28.5 deg (>400 km)	85	9.5	17.0	1.2	2.1
28.5 deg (< 400 km)	207	0.9	1.6	0.1	0.18
39-40 deg	57	1.1	2.4	0.1	0.21
>50 deg (>400 km)	10	2.2	5.2	0.44	1.1
>50 deg (<400 km)	190	1.7	3.8	0.2	0.45
NASA-Mir (51.6 deg x 360 km)	6	50.3	115	0.37	0.84
ISS Exp. 's 1-10 (51.6 deg x 380 km)	13	26.0	68.0	0.16	0.40

Table 5. Calculations of effective doses, %-REID from fatal cancer, and 95% confidence intervals (CI) for lunar or Mars missions. Calculations are at solar minimum where GCR dose is the highest behind a 5-g/cm² aluminum shield. The absorbed dose, *D* and Effective dose, *E* are averaged over tissues prominent for cancer risks. Competing causes of death are considered in the calculation because for high values of risk they compress the risk probabilities (>5%) (Cucinotta and Durante, 2006).

<i>Exploration mission</i> <i>(length of mission)</i>	<i>D, Gy</i>	<i>E, Sv</i>	<i>%-REID</i>	<i>95% CI</i>
Males (40 y)				
Lunar (180 d)	0.06	0.17	0.68	[0.20, 2.4]
Mars swingby (600 d)	0.37	1.03	4.0	[1.0, 13.5]
Mars exploration (1000 d)	0.42	1.07	4.2	[1.3, 13.6]
Females (40 y)				
Lunar (180 d)	0.06	0.17	0.82	[0.24, 3.0]
Mars swingby (600 d)	0.37	1.03	4.9	[1.4, 16.2]
Mars exploration (1000 d)	0.42	1.07	5.1	[1.6, 16.4]

Figure Captions

Fig. 1. The occurrence time of large solar proton events and the time-dependent solar modulation parameter, Φ which describes the modulation of GCR is shown versus calendar year.

Fig. 2. Measurements of the differential lineal energy (y) spectra for GCR (open squares) and total (GCR+trapped) (solid circles) from a TEPC placed in front of phantom torso experiment on ISS Expedition-2 (June 25-July 3, 2001).

Fig. 3. Comparison of calculations of LET and lineal energy spectra to TEPC lineal energy spectra measurements from the GCR and secondaries on the STS-56 shuttle mission.

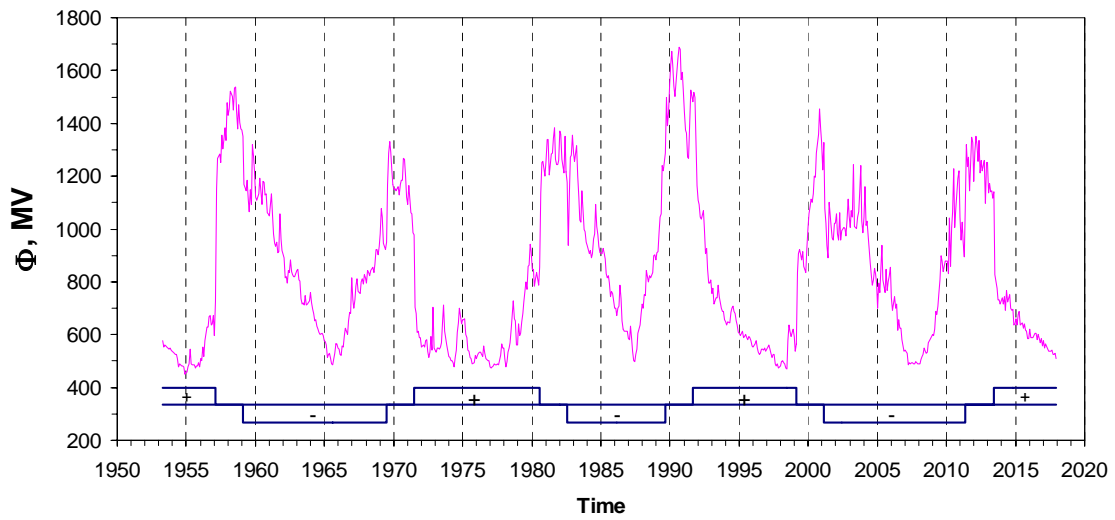
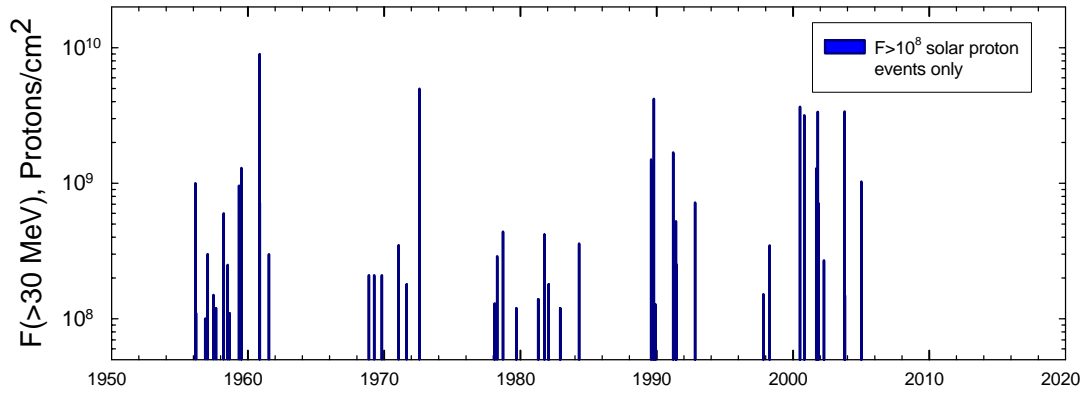
Fig. 4. Calculations from the HZETRN/QMSFRG model for the proton, helium, neutron and heavy ion components to crew doses versus aluminum shielding depth in the ISS orbit.

Fig. 5. The badge doses and effective doses versus calendar year from all astronauts on all NASA space missions (Mercury, Gemini, Apollo, Skylab, Apollo-Soyuz, Shuttle, Mir, and ISS (Expedition 1-10)).

Fig. 6 The effective dose-rates for all NASA space missions (Mercury, Gemini, Apollo, Skylab, Apollo-Soyuz, Shuttle, Mir, and ISS (Expedition 1-10)).

Fig 7. Ratio of total mission dose from TLD-badges for crew-members performing EVA's to crew-members not performing EVA's on same mission. Results show that EVA scheduling to avoid trapped radiation and high Earth magnetic field passes can effectively reduce EVA doses.

Fig. 8. Correlation between physical dosimetry assessment of effective doses relative to biodosimetry from four NASA astronauts from Mir missions, EVA astronauts from STS-103 (Hubble repair mission) and ISS increments. The left-hand panel shows results based on the individuals pre-flight calibration curve to low dose gamma-rays and the right hand panel comparison bases on the population averaged calibration to gamma-rays.



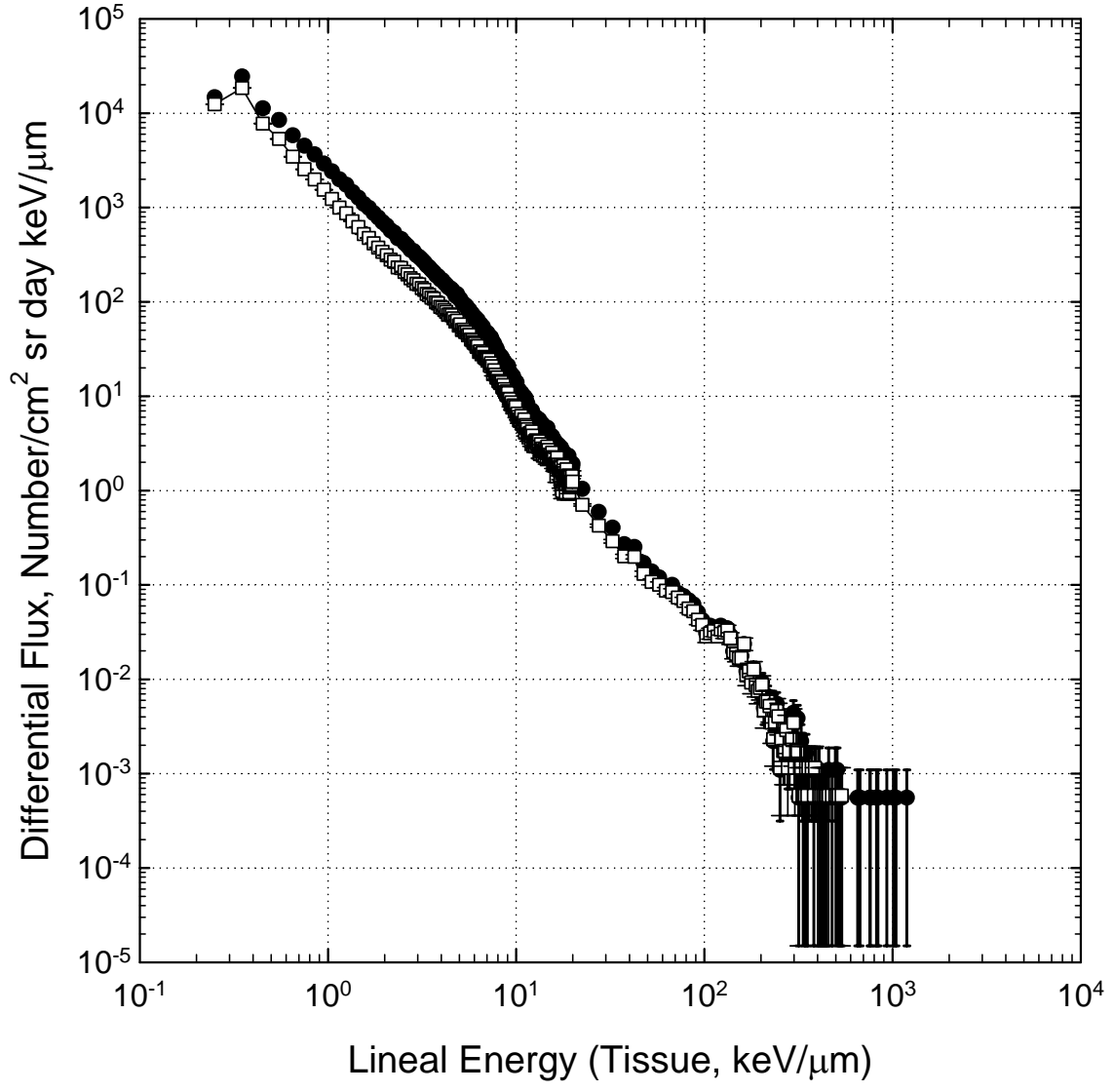


Figure 2

Figure 3

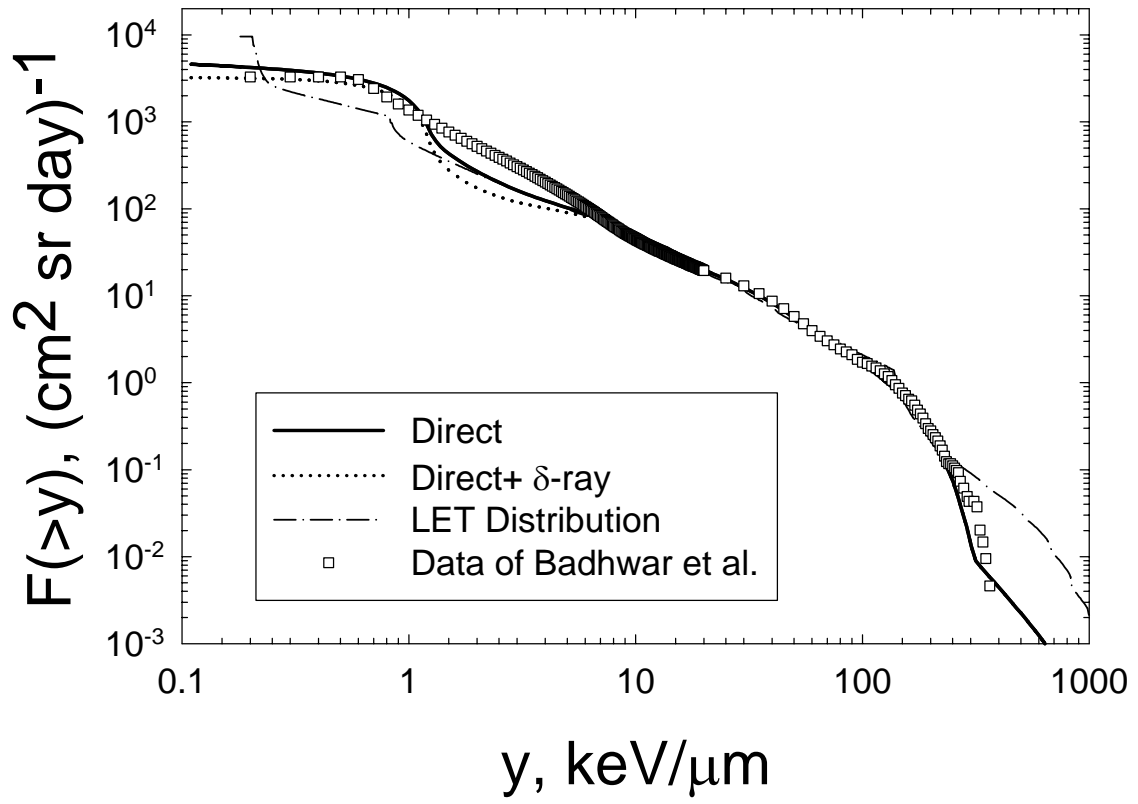


Figure4

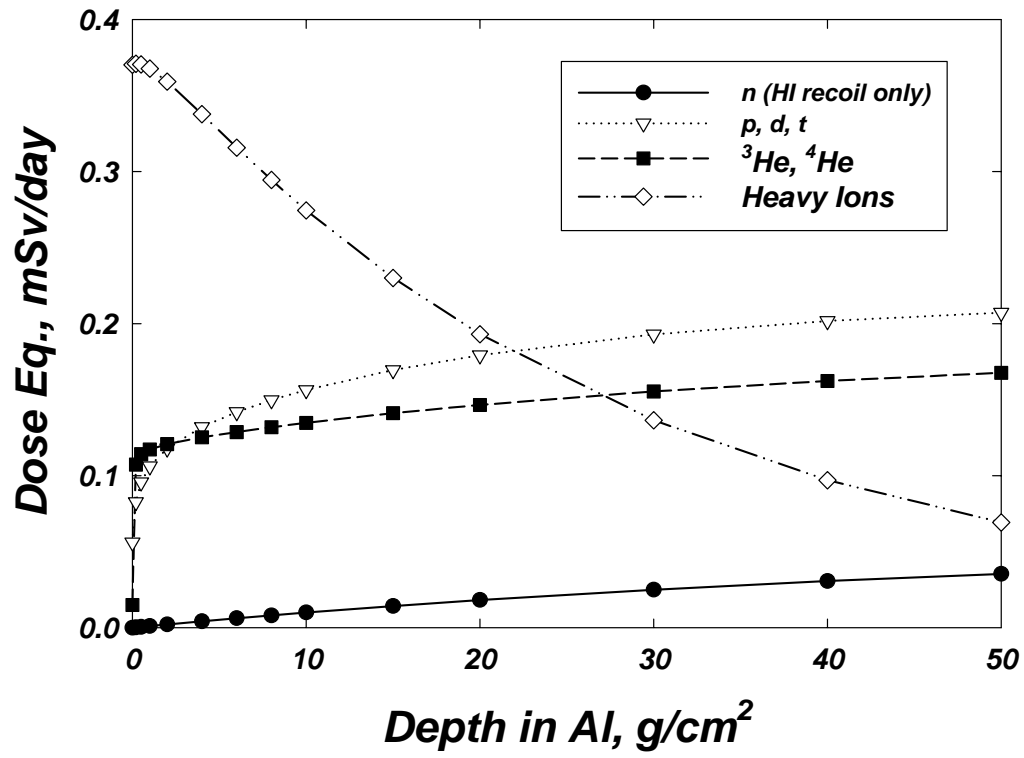
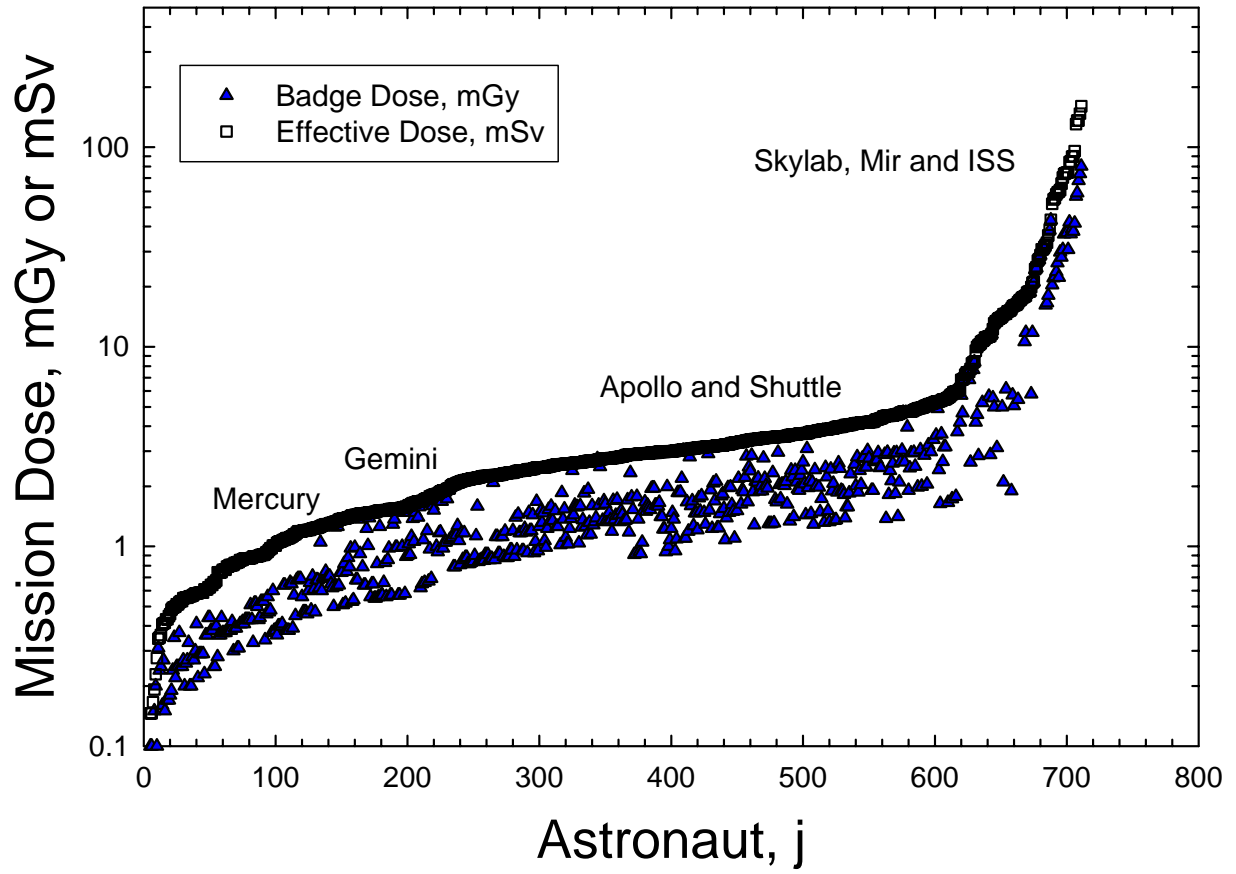


Figure 5



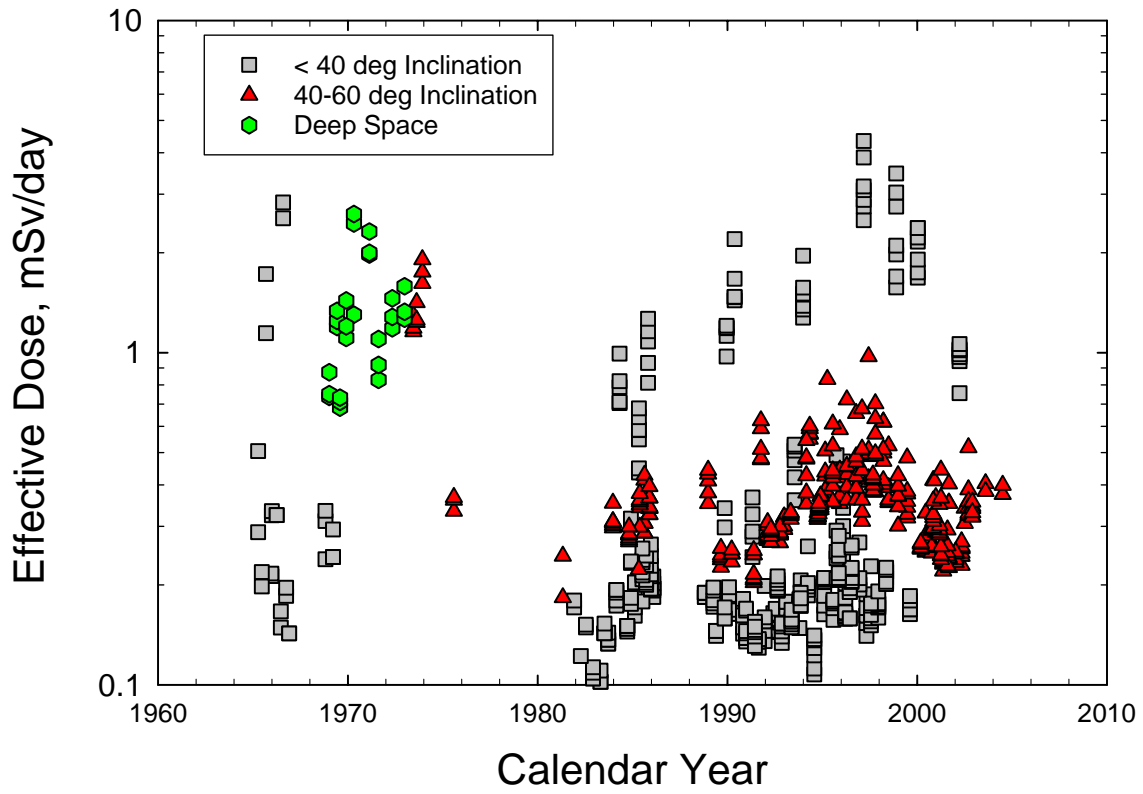


Figure 7

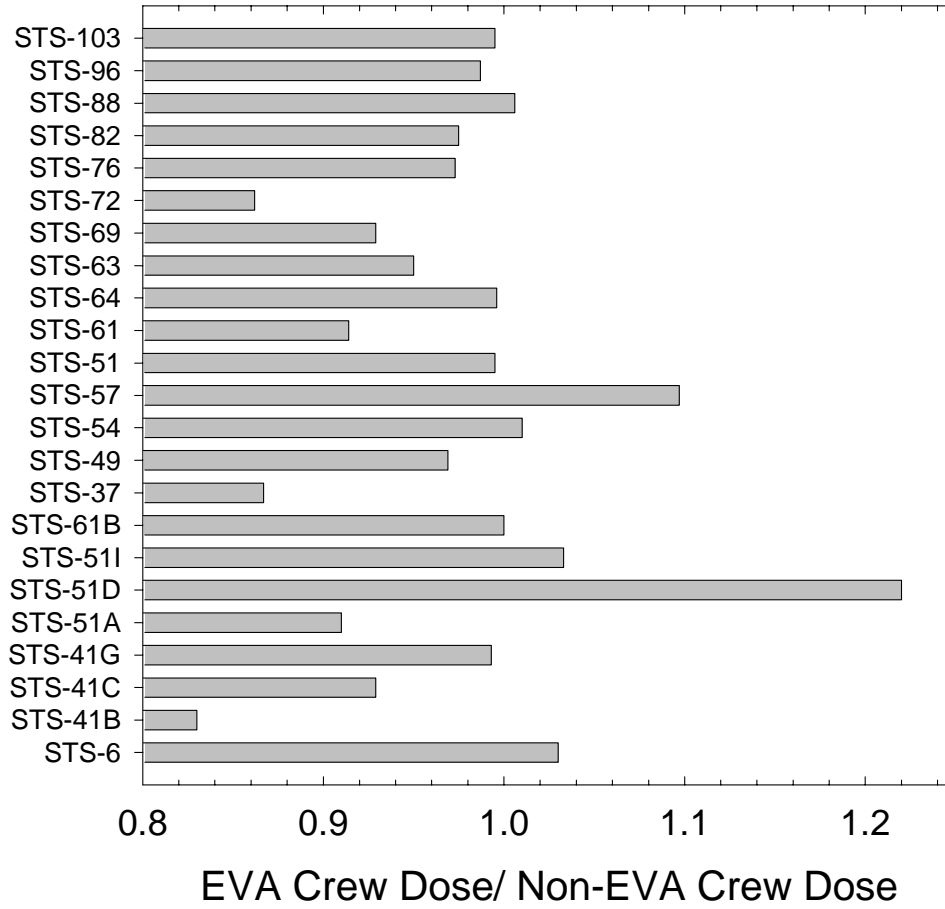


Figure 8

